G. PLASCENCIA*#

# REDUCTION OF INDUSTRIAL NICKEL OXIDES WITH A HYDROGEN BEARING GAS BETWEEN 523 AND 673 K

Reduction of three industrial nickel oxides (Goro, Tokyo and Sinter 75) with a hydrogen bearing gas was revisited in the temperature interval from 523 to 673 K (250 to 400°C). A pronounced incubation period is observed in the temperature interval tested. This period decreases as the reduction temperature increases. Thermogravimetric data of these oxides were fitted using the Avrami-Erofeyev kinetic model. The reduction of these oxides is controlled by a nucleation and growth mechanism of metallic nickel over the oxides structure. Rate kinetic constants were re-evaluated and the activation energy for the reduction of these oxides was re-calculated.

*Keywords:* Nickel oxides reduction; hydrogen reduction; Avrami-Erofeyev kinetic model; nucleation and growth; activation energy.

## 1. Background

Reduction of nickel oxide with hydrogen gas has been extensively studied. Reports on this reaction at different temperatures and hydrogen content in the gas reveal many possible rate limiting steps and kinetics. Different attempts to explain the reduction process have been made, however data not always fit into a unique kinetic model. The different reports clearly demonstrate that it does not exist a unified approach that analytically describes the nickel oxide reduction. Attempts have been made to adjust thermo gravimetric data to well established kinetic models assuming that the data gathered behaves ideally; however, this not always the case and departures from ideality are often found. This approach tends to describe the reaction mechanisms in terms of some kinetic parameters [1]. Even though the same chemical species are used, distinct reaction behaviors are observed, this is not a trivial problem, making this process worthy of research; given its importance in catalysts, fuel cells, among others.

The reduction of some industrial nickel oxides with gases bearing different hydrogen contents at different temperatures has been reported [2-4]. Kinetics of the reduction of these nickel oxides were described using diverse models; the corresponding activation energies were computed as well. The previous results, showed considerable variations under similar testing conditions. Sometimes our results were in good agreement with previous reports, sometimes did not.

Work on the subject matter by Hidayat et. al [5-7] detailed the presence of an incubation period on the reduction of nickel oxides in the temperature range of 573 to 873 K (300 to 600°C). These observations were also made by some other authors [8-10] over the same temperature range.

In addition, Zhou et al [11] surveyed different reports on the reduction of nickel oxide with hydrogen. They reported on the many models that have been used to describe the kinetics of this reduction process. They showed that these models have been formulated solely based on experimental observations and incidentally different reaction mechanisms have been proposed. The vast differences among these models arise from the difficulty in finding out which particular mechanism is responsible for limiting the rate of reduction under given conditions. It has been proposed diffusion controlling mechanisms, chemical reaction mechanisms and even mixed controlled kinetics.

Jancovic et al. [12,13] also studied the reduction of nickel oxide with hydrogen from room temperature to 773 K (500°C) under variable temperature conditions, using different heating rates. To describe the kinetics of nickel oxide reduction they tested different kinetic models; eventually, they described the reduction process using the Sestak-Berggen model, which utilizes four kinetic variables determined directly from TGA data. They concluded that nickel metal forms directly at the metal/oxide interface.

Based on these observations, it was decided to revisit our own data on the reduction of industrial nickel oxides between 523 and 673 K (250-400°C), using a reducing gas containing hydrogen (35 %volume) and argon (grade 5.0, balance). The aim of this report is to propose a possible mechanism for the reduction of nickel oxide at these temperatures and relate it to the best fitting kinetic law.

* CIITEC-INSTITUTO POLITÉCNICO NACIONAL, CERRADA CECATI S/N, CD. DE MÉXICO, C.P. 02250, MÉXICO
# Corresponding author: g.plascencia@utoronto.ca

782

## 2. Experimental

### 2.1. Materials

Three industrial nickel oxides were tested: Goro, Tokyo and Sinter 75. Goro nickel oxide is obtained by oxidizing nickel chloride slurries in a fluidized roaster. Nickel oxide layers successively grow by vapour deposition, resulting in a nearly spherical geometry with some porosity between oxide layers. Tokyo and Sinter 75 nickel oxides are obtained by fluid-bed roasting of nickel sulphide pellets.

#### 2.1.1. Oxides characterization

The chemical composition of the nickel oxides was obtained using a Thermo Elemental (VG) PlasmaQuad PQ ExCell ICP-MS analyser coupled to a Nu-wave UP 213 laser ablation microscope. Sulphur was analyzed using a LECO CS600 carbon and sulphur analyzer. The density of each oxide was measured in a Scott volumeter (ASTM B 329). BET surface area for these nickel oxides was determined using a Monosorb™ surface area analyzer. Chemical composition, density and BET surface area of the oxides are shown in Table 1.

The density of each oxide is very close to the theoretical value of 6670 kg/m$^3$. The size distribution of each oxide sample has been already reported [4]. Regardless of its origin, nickel oxide particles are between 300 and 600 mm. Less than 7% was greater than 1.2 mm. This reflects in the BET surface area measurements.

Figure 1 shows micrographs of the different nickel oxides tested. Goro nickel oxide particles exhibit the most well defined geometry; each oxide particle can be described as either, a sphere or an ellipsoid; whereas the Tokyo oxide particles look like irregular flat disks, and the Sinter 75 oxide resembles a random aggregate of particles. As a consequence of these morphological features, several micro-cracks and pores develop in each oxide particle. Because of the differences in chemical composition and morphology, it is not expected that reduction kinetics of these oxides be identical under the same conditions.

### 2.2. Reduction tests

Reduction tests were conducted in a thermal gravimetric analysis unit (SETARAM TGA-92) with detection limit of 10 mg at a constant heating rate of 10°C/min. The samples used in the reduction experiments were around 115 mg ±5 mg. The samples were heated in alumina crucibles under an argon (99.999% Ar, $H_2O$ < 2ppm, $O_2$ < 2 ppm, THC < 0.5 ppm) atmosphere. Once the test temperature was reached, the inert gas was switched off and the reducing gas consisting of a hydrogen (99.9995% $H_2$, $H_2O$ < 1 ppm, $N_2$ < 1 ppm, $O_2$ < 0.5 ppm) – argon mixture with 35 volume% of hydrogen was allowed into the reaction chamber. To avoid any sort of gas transport, the gas reducing gas flowed at 500 mL/min. The experiments were conducted between 523 and 673 K (250 and 400°C). The reproducibility of the tests was within ±5%.

TABLE 1

Chemical assays, density and BET surface area of the nickel oxides tested

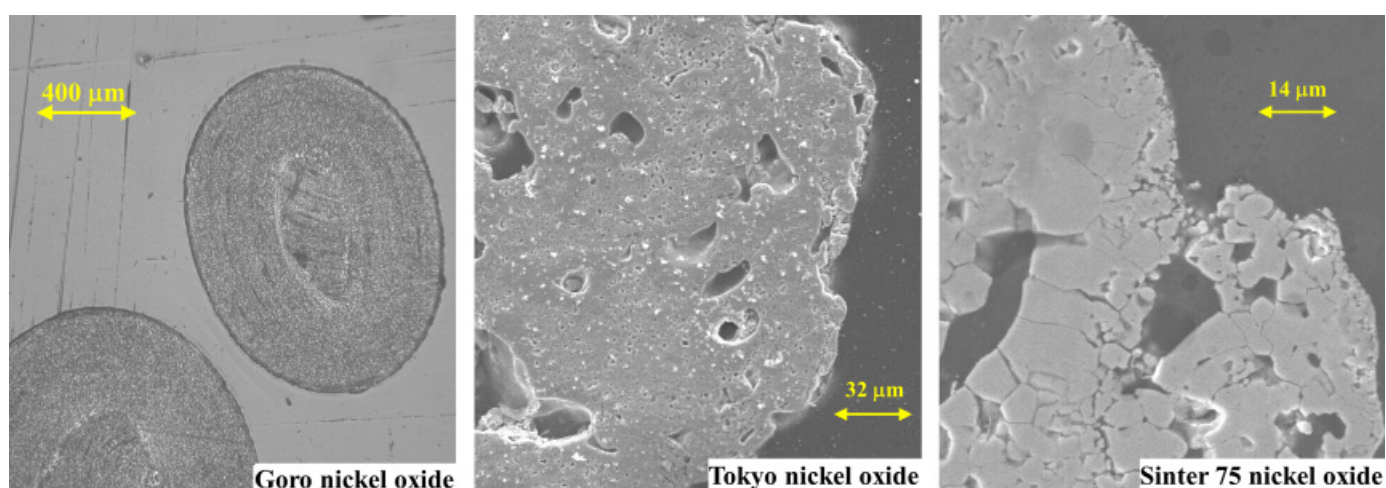| Oxide sample | Chemical composition, [mass %] | | | | | | | | | | Density [kg/m$^3$] | BET [m$^2$/g] |
|---|---|---|---|---|---|---|---|---|---|---|---|---|
| | Ni | Cu | Co | Fe | Ca | Al | Mg | Si | Pb | S | | |
| Goro | 80.3 | 0.03 | 0.36 | 0.20 | 0.024 | 0.039 | 0.04 | 0.040 | 0.022 | 0.013 | 6550 | 0.023 |
| Tokyo | 75.3 | 0.14 | 1.15 | 0.54 | 0.054 | 0.026 | 0.12 | 0.024 | 0.061 | 0.006 | 6650 | 0.071 |
| Sinter 75 | 76.1 | 0.80 | 0.84 | 0.64 | 0.143 | 0.224 | 0.04 | 0.453 | 0.124 | 0.007 | 6540 | 0.051 |



Fig. 1. SEM micrographs of the Goro (a), Tokyo (b) and Sinter 75 (c) nickel oxides

### 3. Results

Figures 2a to 2c show the percentage of mass lost by the nickel oxides tested as a function of time when reduced under the cited conditions. At the lowest temperature, reduction of the oxides is extremely slow, taking a considerable amount of time before the metallic nickel begins to form on the exposed oxide surface. As the testing temperature is increased, the reduction process accelerates. To achieve full oxide reduction, the nickel oxide sample should lose 21.41% of its initial mass; however, it is clear from the plots that such figure is far from reaching.

The maximum mass lost recorded is about 18% for the Tokyo batch at 623 K (350°C) after nearly 2.5 hours of exposure to the reducing gas. The same oxide batch was tested at 673 K (400°C), but the experiment was stopped after 30 minutes; the trend shown in the data suggests that at this temperature, the oxide would reach a similar weight loss as that at 623 K but in a considerable shorter time. The reduction rates exhibited by the Tokyo oxide are similar to those presented by the Sinter 75 oxide. On the other hand, the Goro sample reduces at a slower rate than the other two oxide samples.

The reduction rates observed in this temperature interval are slower compared to those found on the same samples when reduction experiments were conducted at higher temperatures [2-4]. The reduced fraction ($\alpha$) of the nickel oxides was computed to find out the mechanism responsible for the reduction kinetics in the interval tested. This fraction is defined as:

$$\alpha = \frac{\% \, mass \, lost}{21.41} \quad (1)$$

Figures 3 a to c shows the reduced fraction for the different oxides tested as a function of reducing time. It can be seen in these figures how far from achieving full conversion are these experiments; the lower the temperature the slower the oxides reduction. Moreover, it is evident that the three oxides, need a very long exposure time to the reducing gas at 523 K (250°C) before reduction takes place. As temperature increases, this initial "incubation" period shortens drastically.

At 673 K (400°C) it is observed that the incubation period still is present for the oxides, however its duration has considerably reduced compared to the period exhibited at 523 K.
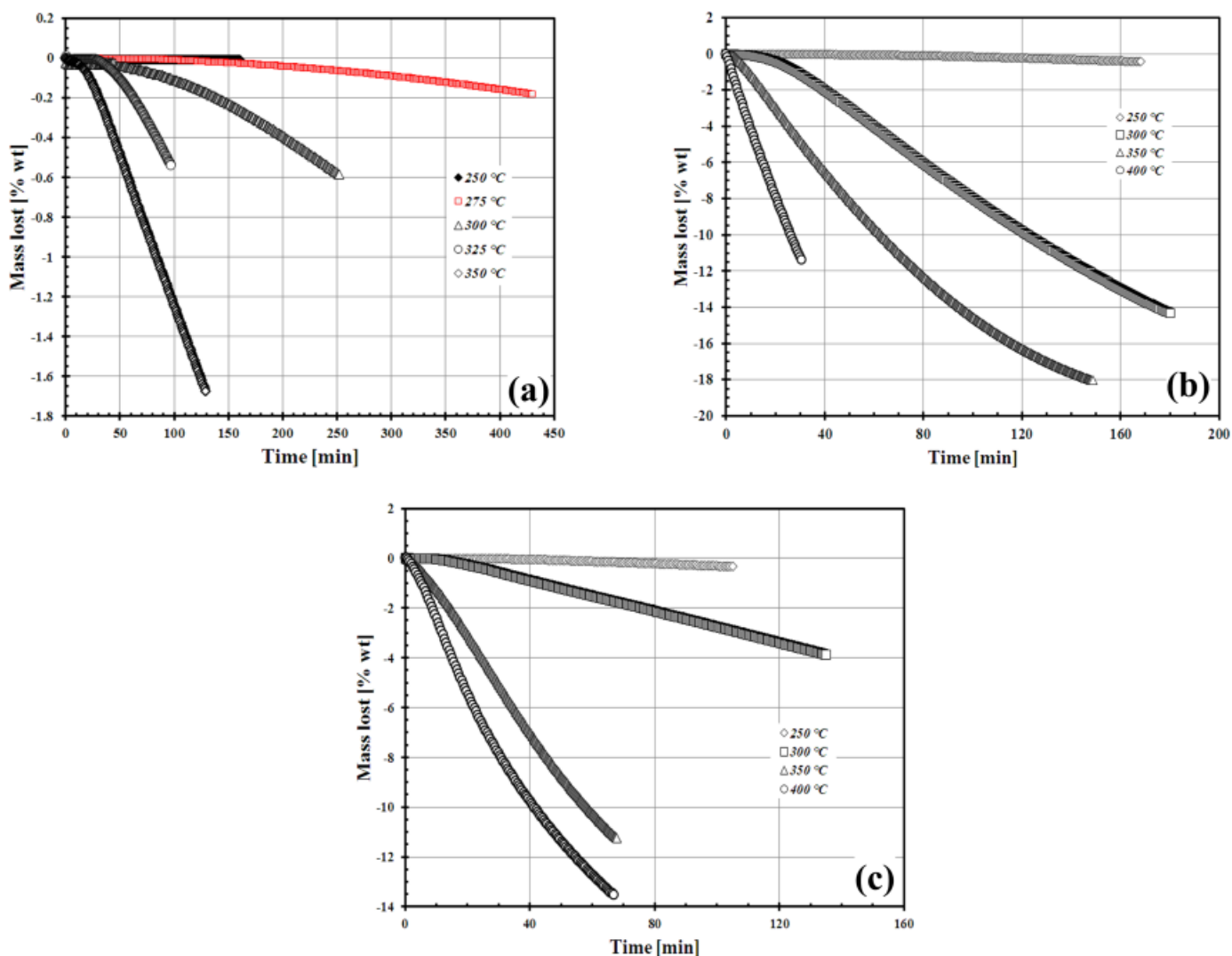


Fig. 2. Nickel oxide mass lost (wt%) as a function of time between 523 and 673 K (250 and 400°C) in a gas containing 35%vol $H_2$ for (a) Goro nickel oxide, (b) Tokyo nickel oxide and (c) Sinter 75 nickel oxide
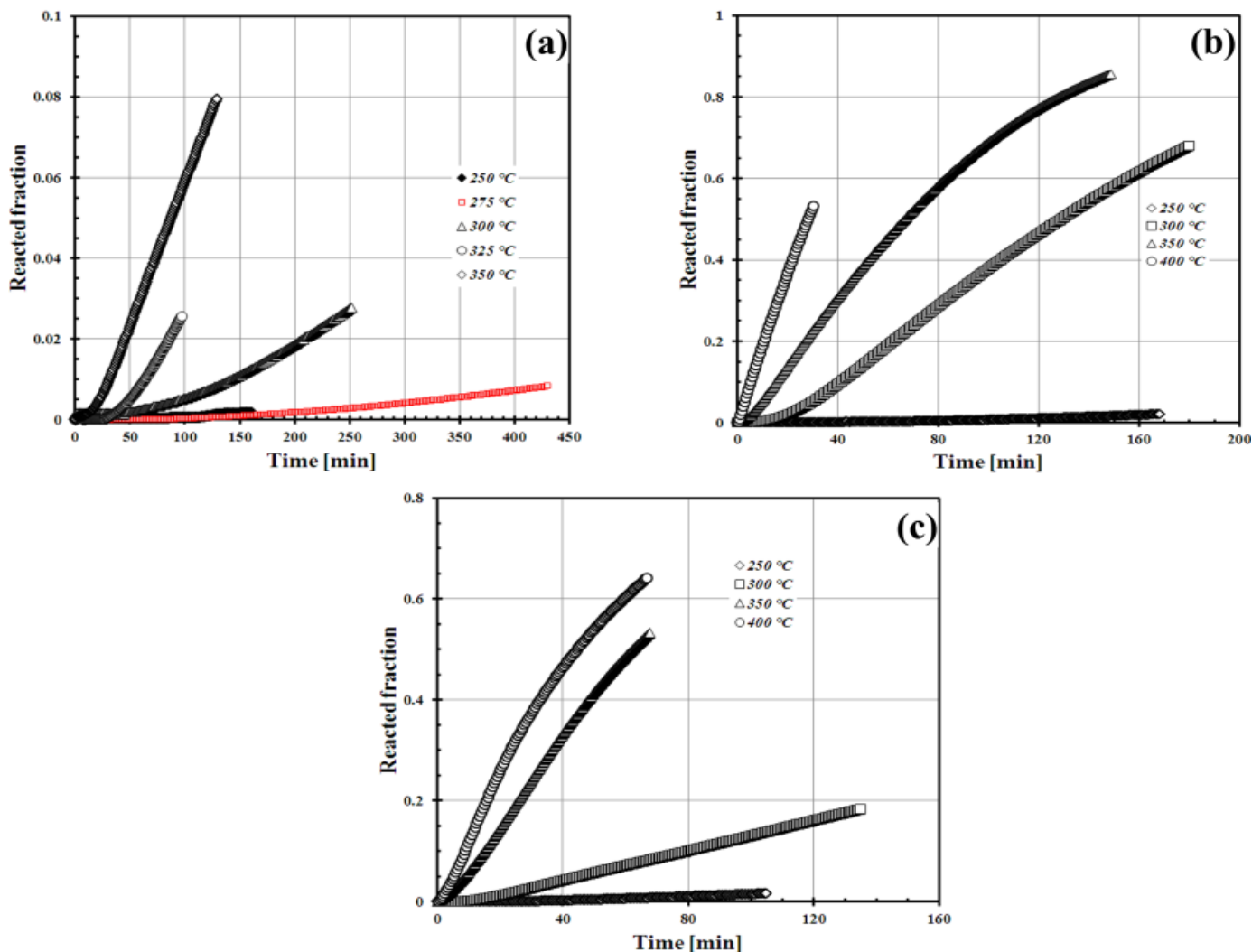
Fig. 3. Reacted fraction during the reduction between 523 and 673 K (250 and 400°C) in a gas containing 35%vol H$_2$ of (a) Goro oxide, (b) Tokyo oxide and (c) Sinter 75 oxide

Higher values for the reduced fraction occur at higher test temperatures (673 K for Tokyo and Sinter 75, 623 K for Goro). It is required considerable exposure time to the gas to start obtaining a little amount of nickel metal form the oxides. The three oxides behave similarly under the same experimental conditions.

The Goro sample when heated up to 623 K (350°C) shows a reduction rate that would require little more than 24 hours to achieve full reduction. The Tokyo oxide exhibits faster reduction rates than those shown by the Goro samples at the same testing temperatures. The Sinter 75 batch shows the fastest reduction rate of the oxides tested.

At 523 K (250°C), the three commercial oxide batches remain practically un-reacted even after two hours of exposure to the reducing gas. Independent reduction tests at this temperature on the Goro sample with increased hydrogen content in the reducing gas showed no improvement over the reduction rate of this oxide at this temperature.

Comparing these sets of data with the results previously obtained at higher temperatures, it is clear the marked effect that temperature has on the rate of reduction for these oxides. Results presented by different authors show the same trend.

It was concluded [2-4] that the rate of reduction sharply increases for these three oxides when the test temperature was raised to about 873 K (600°C). It was found that the Goro oxide reduces following to the topo-chemical model [3], whereas the Tokyo and Sinter 75 oxides reduce following a combined mechanism [4], that can be approached by the grain model proposed by Szekely et al [14].

Figure 4 shows the extent of reduction for the three oxides at 523 and 623 K (250 & 350°C). From this figure, it is clear that Goro oxide shows the lowest reduction rate. The Goro sample reduces at a rate two orders of magnitude slower than those exhibited by the Tokyo and the Sinter 75 samples. At 623 K (350°C) the rate of reduction of Tokyo and Sinter 75 oxides is virtually the same. At 523 K (250°C), the Sinter 75 batch reduces faster than the Tokyo oxide.

The irregularity in geometry and also structural features like cracks and pores of the Tokyo and Sinter 75 batches may provide sites for rapid transport of hydrogen within the oxide structure, easing the reduction process in these oxides. On the other hand, the compact layered structure of the Goro sample may provide some sort of diffusion barrier for the dif-
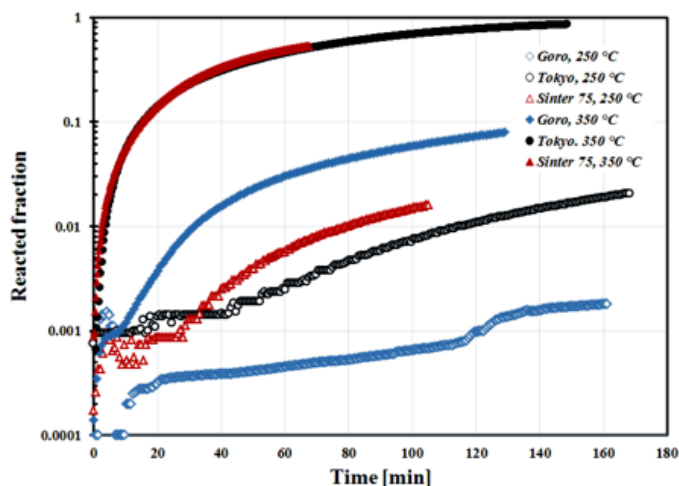
Fig. 4. Reduction of the nickel oxide samples at 523 and 623 K (250 and 350°C)

fusion of hydrogen that renders the ability of the gas to reduce this oxide.

## 4. Discussion

To find out the possible reduction mechanism, Zhou et al. [11], proposed the use of the general kinetic equation:

$$\ln\left(-\ln\left(1-\alpha\right)\right) = \ln\left(a\right) + n_{AE}\ln\left(t\right) \qquad (2)$$

Where $\alpha$ is the reacted fraction, $t$ is the reduction time [s], a is a constant and $n_{AE}$ is the Avrami-Erofeyev exponent.

Plotting the kinetic data measured in the form of $\ln(-\ln(1-\alpha))$ vs. $\ln(t)$, should give linear plots whose slopes reveal the value of n in equation (1). If $n_{AE} < 1$, it means that the reduction process is diffusion controlled, whereas if $n_{AE} \approx 1$, a phase-boundary mechanism is likely to control the oxide reduction. Figures 5 a to c show these plots.

It can be seen in these plots that as the test temperature increases, a more linear response is obtained; however, at temperatures below 623 K (350°C), the incubation period observed in the three oxides does not allow for having a good fit of the data. However, these plots again reveal the important effect that temperature has on the reduction of these industrial oxides.

These observations are in good agreement with those already made [8]; furthermore, the data shown in figure 3 a to c clearly indicate the existence of an induction (i.e. nucleation) period that seems to depend on the nature of the sample (morphology, texture, processing) and test temperature. Regarding to the former, the presence of defects (at micro and macro scales) somehow must affect the beginning of incubation period. The presence of impurities, vacancies and even the pre-treatment of the oxide samples have an effect on the rate of reduction reaction; since the reaction takes place at the gas/oxide interface [15]. The reduction rate is proportional to that interfacial area.

Independently, Delmon and Roman [16] noticed that reducing nickel oxide below or above the Néel temperature ($T_N$) of
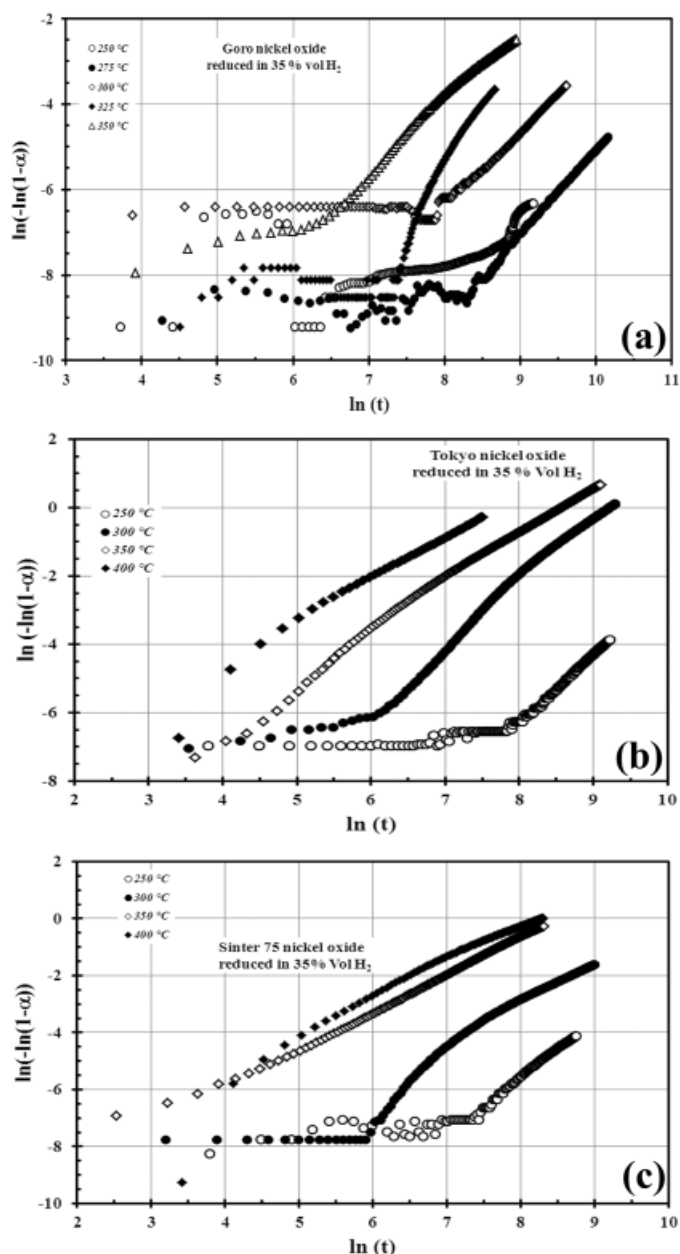






Fig. 5. Plots of $\ln(-\ln(1 - \alpha))$ vs $\ln(t)$ for the reduction of (a) Goro oxide, (b) Tokyo oxide and (c) Sinter 75 oxide

the oxide (252°C) affects its rate of reduction. It was found that below $T_N$, more Ni nuclei develop, thus increasing the length of the incubation period.

Later on, in situ experimental observations made independently by Richardson et al. [15], Jeangros et al. [17] and by Manukyan et al. [18], revealed that in the experimental temperature range reported in this work, confirms that reduction of nickel oxide occurs by a nucleation and growth mechanism.

Richardson et al. [15], proposed that nickel oxide reduction occurs in three stages:

1) Metallic nickel appears as isolated clusters during the incubation period, as hydrogen dissociates around oxygen vacancies.

2) The rate of reduction increases as the initial metal clusters grow due to an autocatalytic effect.

3) The system achieves steady state and the reduction proceeds until the oxide disappears. The presence of water vapour (reaction product) on the nickel surface may slow down the reduction reaction.

High resolution TEM microscopy [17] shows that nickel metal grows epitaxially over the oxide after metal nucleation on the oxide even at temperatures below 673 K (400°C). It was observed that as the nickel nucleates, NiO grains shrink due to the oxygen loss, creating pores and becoming irregular as they get reduced. The unreacted oxide grains remain unchanged.

Manukyan et al. [18], concluded that in the temperature interval from 543 to 773 K (270 to 500°C), incomplete reduction of nickel oxide results in a complex porous structure. This structure results from slow nickel nucleation rate and outward diffusion of water vapour molecules. When temperature is incremented, the amount of nickel nuclei significantly increases, allowing for faster reduction rates.

SEM observations [6] on nickel oxide specimens exposed to pure hydrogen at 573 K (300°C) revealed that upon reduction, nickel metal has a flake like structure. The nickel flakes are separated by crevices presumably created during the initial nucleation of the metal phase. The cracks seem to facilitate gas transport towards the reaction sites. When temperature is increased, these nickel flakes become finer.

These findings [6,15,17,18] agree with observations by Rodríguez et. al [19], after reducing NiO (1 0 0) oriented crystals as well as NiO powders. They found between 523 and 623 K (250 and 350°C) the presence of an incubation period. During this period, nickel oxide reduces directly to nickel metal; as this happens, defect sites form on the oxide surface. These sites aid on the dissociation of $H_2$ molecules. Of the defects, oxygen vacancies allow for an increase in hydrogen adsorption, lowering the energy barrier associated to this process. In addition, the adsorbed hydrogen helps inducing oxygen vacancies from the oxide bulk towards its surface. Thus metal nucleation strongly depends on the removal of oxygen from the oxide, becoming the rate limiting factor only if there is enough dissociated hydrogen on the oxide surface. This agrees with Richardson's findings [15].

Based on these observations, it seems plausible that a nucleation and growth rate mechanism is responsible for controlling the rate of reduction of the industrial nickel oxides tested in this work.

Figure 6 shows a SEM image of a partially reduced Goro oxide particle at 623 K (350°C). From this image it can be noticed the reaction interface. The nickel product develops from the outer side of the oxide particle towards its core. It can be seen higher porosity in the metallic nickel region (outer part) of the reduced particle. The porosity decreases when moving into the particle's centre. This would mean that hydrogen diffusion in the oxide is faster, particularly at the beginning of the reduction reaction. As the hydrogen tries to penetrate into the denser oxide, the diffusion slows down, retarding the reaction. This goes in hand with the incubation period. Even more, this may suggest that in order to proceed to full oxide reduction, the metal phase has to nucleate on the oxide surface. The structure of the reduced

nickel is fairly smooth and fine. There appears to be some oxide particles embedded in the fine nickel metal matrix.
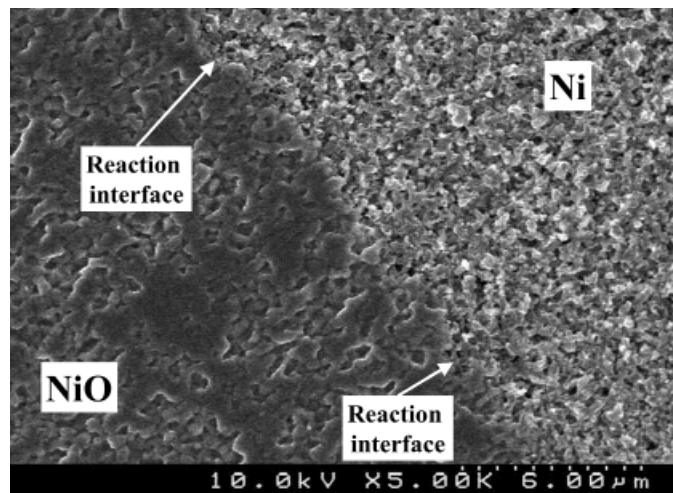


Fig. 6. Image of a partially reduced Goro oxide particle at 623 K (350°C)

Because of this, the experimental data was re-fitted using an Avrami-Erofeyev kinetic model [19]:

$$kt = \left[ -\ln\left(1 - \alpha\right) \right]^{\frac{1}{n_{AE}}} \qquad (3)$$

where $k$ is the kinetic rate constant, $t$ is time [s], $\alpha$ is the reacted fraction and $n_{AE}$ has to be found from experimental data. After testing the model, it was found that the value of $n_{AE}$ that offers the best fit for the Goro and Sinter 75 oxide samples is 1; whereas for the Tokyo oxide batch, $n_{AE} = 1.5$. Figures 7 a to c, shows the experimental data fitted to equation (3).

These results confirm that at the temperature interval tested, nickel oxide reduces with hydrogen gas due to a chemical reaction mechanism at the metal-oxide interface. This is in good agreement with Zhou's [11] model predictions and microscopic observations made [6,15,17,18].

The data plotted in figures 7 a to c show a strong lineal trend, therefore it is assumed that the observed values for $n_{AE}$ are correct. Rising $n_{AE}$ to 2 and higher values results in an increasing departure form linearity, especially at greater test temperatures. The slope of the curves in figures 7 a to c represents the rate constant which is used to estimate the activation energy of oxide reduction in the reported temperature interval. The values of such constants are shown in Table 2, along with the correlation coefficient found during data fitting.

The activation energy for the reduction of the three nickel oxide samples was calculated using Arrhenius equation:

$$k = A\exp\left(-\frac{E_A}{RT}\right) \qquad (4)$$

where $k$ is the rate constant, $A$ is a constant, $E_A$ is the activation energy [kJ/mole], $R$ is the universal gas constant [8.314 J/mole/K] and $T$ is the absolute temperature [K].
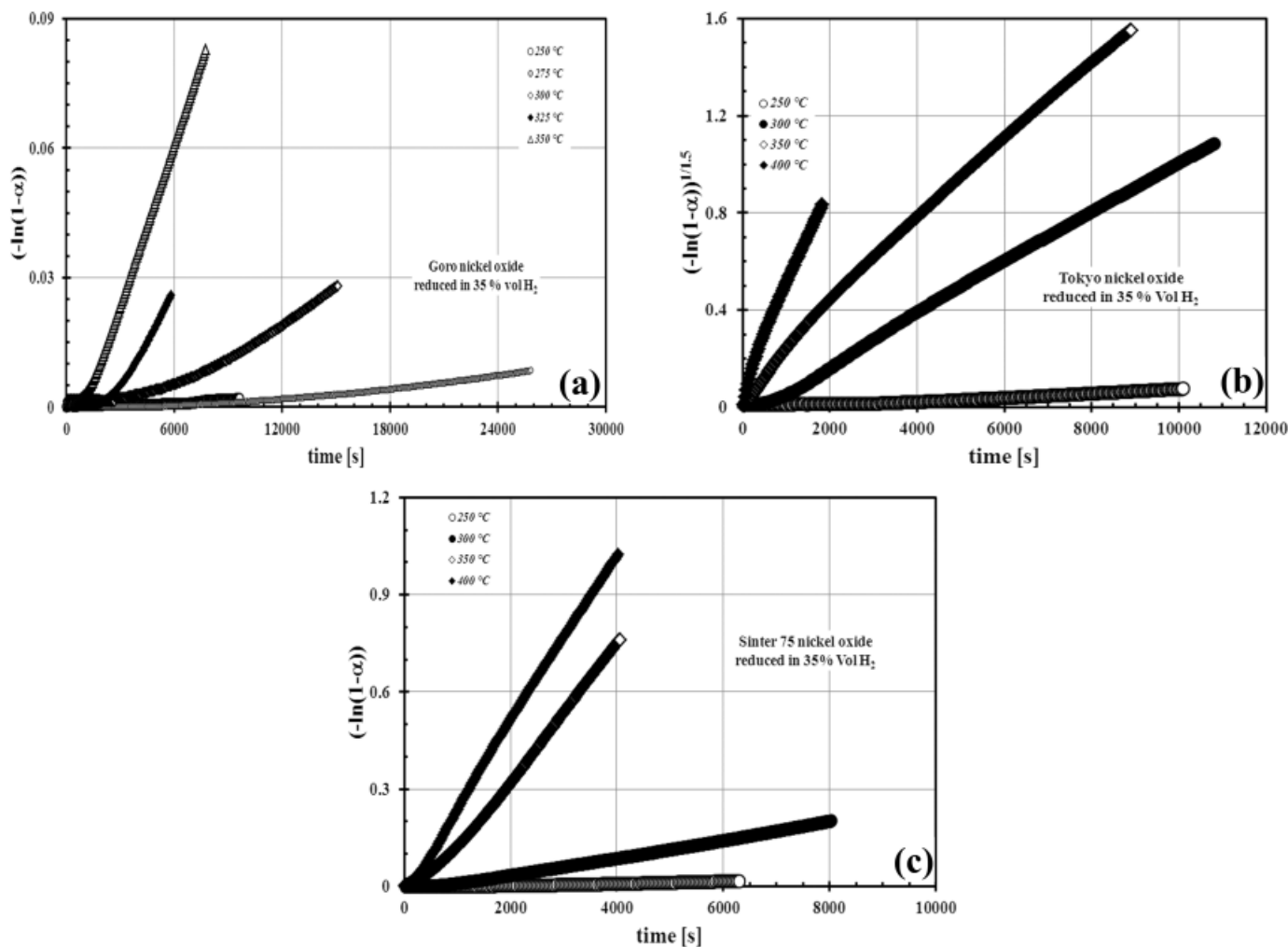
Fig. 7. Estimation of kinetic rate constants using the second order Avrami-Erofeyev kinetic model for (a) Goro oxide, (b) Tokyo oxide and (c) Sinter 75 oxide

TABLE 2

Kinetic rate constants for Goro, Tokyo and Sinter 75 nickel oxide samples. Correlation coefficients for each constant are shown in parenthesis

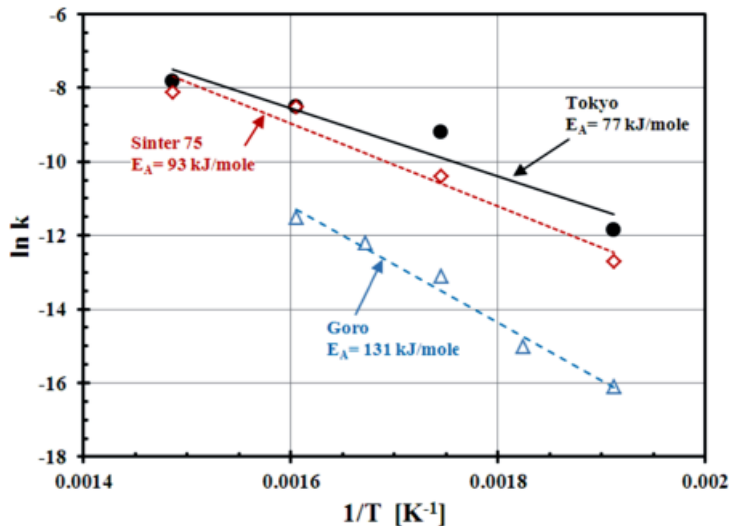| Temperature [°C] | k | | |
|---|---|---|---|
| | Goro | Tokyo | Sinter 75 |
| 250 | $10^{-7}$ ($r^2 = 0.9499$) | $7 \times 10^{-6}$ ($r^2 = 0.9582$) | $3 \times 10^{-6}$ ($r^2 = 0.9363$) |
| 275 | $3 \times 10^{-7}$ ($r^2 = 0.9368$) | | |
| 300 | $2 \times 10^{-6}$ ($r^2 = 0.9344$) | $10^{-4}$ ($r^2 = 0.9989$) | $3 \times 10^{-5}$ ($r^2 = 0.9956$) |
| 325 | $5 \times 10^{-6}$ ($r^2 = 0.8898$) | | |
| 350 | $10^{-5}$ ($r^2 = 0.9904$) | $2 \times 10^{-4}$ ($r^2 = 0.9967$) | $2 \times 10^{-4}$ ($r^2 = 0.9938$) |
| 400 | | $4 \times 10^{-4}$ ($r^2 = 0.9918$) | $3 \times 10^{-4}$ ($r^2 = 0.9991$) |



Fig. 8. Activation energy for the reduction with hydrogen bearing gas of Goro, Tokyo and Sinter 75 nickel oxides in the temperature interval of 523 to 673 K (250 to 400°C)

Figure 8 shows the plot of ln(k) vs 1/T for the three oxides tested. Table 3 shows the activation energy for the reduction of these oxides, and its comparison with other published reports.

As it can be seen in Table 3, there are some discrepancies in the reported activation energy. These differences may arise from

788

two sources: the first being the nickel oxide itself (processing, impurity level, particle size) and the second, how the thermo-gravimetric data was processed i.e., which kinetic model was chosen to fit the data and how good the fit was. This last issue has been pointed out recently by L'vov [21], whom discussed this traditional data fitting to describe solid-gas reactions. L'vov used a thermochemical approach to describe reactions such as that of nickel oxide reduction with gaseous species. The use of this approach seems to offer activation energies higher than those obtained in previous reports.

TABLE 3

Activation energy for the nickel oxide samples tested and its comparison with previous reports

| Reference | *Ea* [kJ/mole] | Temperature interval [°C] |
|---|---|---|
| This work | 131 (Goro) 77 (Tokyo) 93 (Sinter 75) | 250-350 250-400 250-400 |
| Parravano [9] | 110 | 155-200 |
| Richardson et al [15] | 127 | 210-310 |
| Jeangros et al [16] | 79 | 300-600 |
| L'vov [20] | 175 | 201-225 |

It was previously reported [3] that Tokyo and Sinter 75 have activation energies between 23 and 32 kJ/mole. In this new report such values have changed considerably. The changes in this value obey: firstly in this paper we only focused on the low temperature interval and secondly we used a different kinetic model to describe the reduction process. By considering the reduction of these oxides at higher temperatures, the activation energies reported were lower than those reported at this time. However the activation energy values found for the three oxides in the temperature interval texted are within the different values reported elsewhere.

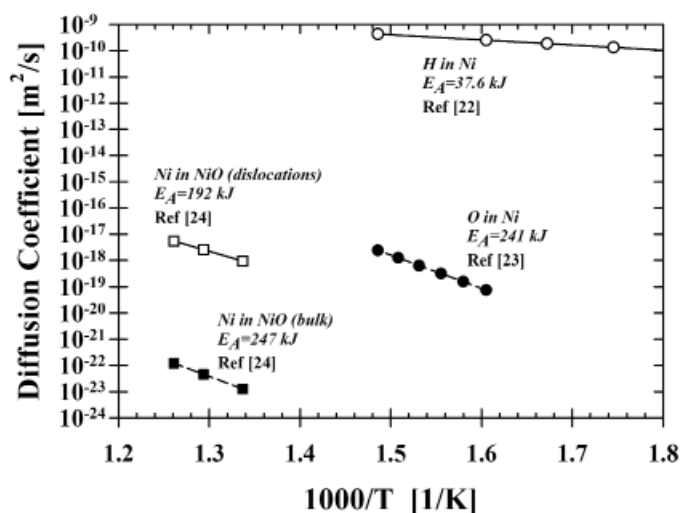Additionally, the diffusivities of hydrogen in nickel [22], oxygen in nickel [23] and nickel in NiO [24] within the testing temperature interval, show that hydrogen diffuses faster than oxygen in the metal. Nickel diffusion in the oxide is favored by five orders of magnitude when the metal diffuses through dislocations at the oxide grain boundaries. If nickel diffuses over the NiO lattice, its diffusion slows down considerably. Figure 9, shows these diffusivities along with their respective activation energies. From this figure, it can be seen that the activation energy for the diffusion of hydrogen in Ni (36 kJ/mole) is at least a half of that for the reduction of Tokyo oxide and nearly 3.5 lower than that for the reduction of Goro oxide. This may also help explaining the presence of the incubation period. While the hydrogen readily diffuses, it takes some time to reach the energy to start reducing the oxide molecule.

## 5. Conclusions

Reduction kinetics of three industrial nickel oxides between 523 and 673 K (250 and 400°C) with a hydrogen bearing gas are reported. It was found that an incubation period occurs. As the test temperature increases, the incubation period decreases, accelerating the reduction rate of the oxides. During the incubation period, structural defects in the nickel oxide, i.e. oxygen vacancies may be responsible for starting the reduction process, as these defects provide sites for the nucleation of nickel metal. As the test temperature increased the easier it becomes for the oxide to create more of these defects, accelerating the reduction kinetics.

Under the experimental conditions, the reduction of the oxides tested is controlled by nucleation and growth of nickel metal on the oxide structure. The activation energy for the reduction of these oxides varies from 77 kJ/mole (Tokyo oxide) to 131 kJ/mole (Goro oxide). These differences may arise from the disparities in chemical composition and the structure and morphology of these nickel oxides. Consequently, it should be considered the processes to obtain these materials to achieve full oxide reduction in a short period of time. It is desirable (industrially) to maximize the metallic nickel production with minimum adjustments to operating parameters; among them, pre-treatment of the oxides, residence time and temperature in the reactor, reducing gas composition and flow rate, among others.

Fig. 9. Diffusivity of H in Ni [22], O in Ni [23] and Ni in NiO [24] over the test interval

## REFERENCES

[1] N. Koga, J. Malek, J. Sestak, H. Tanaka, Netsu Sokutei. **20**, 210-223 (1993).

[2] T.A. Utigard, G. Plascencia, T. Marin, J. Liu, A. Vahed, M. Muinonen, Can. Met. Q. **44**, 421-428 (2005).

[3] T.A. Utigard, M. Wu, G. Plascencia, T. Marin, Chem. Eng. Sci. **60**, 2061-2068 (2005).

[4] G. Plascencia, T. Utigard, Chem. Eng. Sci. **64**, 3879-3888 (2009).

[5] T. Hidayat, M.A. Rhamdhani, E. Jak, P.C. Hayes, Met. Mater. Trans. B. **40B**, 1-16 (2009).

[6] T. Hidayat, M.A. Rhamdhani, E. Jak, P.C. Hayes, Met. Mater. Trans. B. **40B**, 462-473 (2009).

[7] T. Hidayat, M.A. Rhamdhani, E. Jak, P.C. Hayes, Met. Mater. Trans. B. **40B**, 474-489 (2009).

[8] A. Benton, P. Emmett, J. Am. Chem. Soc. **46**, 2728-2737 (1924).

[9] G. Parravano, J. Am. Chem. Soc. **74**, 1194-1198 (1952).

[10] Y. Iida, K. Shimada, Bull. Chem. Soc. Jpn. **33**, 1194-1196 (1960).

[11] Z. Zhou, L. Han, G.M. Bollas, Int. J. Hydrogen Energy **39**, 8535-8556 (2014).

[12] B. Jankovic, B. Adnadevic, S. Mentus, Thermochim. Acta **456**, 48-55 (2007).

[13] B. Jankovic, B. Adnadevic, S. Mentus, Chem. Eng. Sc. **63**, 567-575 (2008).

[14] J. Szekely, C.I. Lin, H.Y. Sohn, Chem. Eng. Sci. **28**, 1975-1989 (1973).

[15] J.T. Richardson, R. Scates, M.V. Twigg, Appl. Catal. A. **246**, 137-150 (2003).

[16] B. Delmon, A. Roman, J. Chem. Soc. Faraday Trans. I. **69**, 941-948 (1973).

[17] Q. Jeangros, T.W. Hansen, J.B. Wagner, C.D. Damsgaard, R.E. Dunin-Borkowski, C. Hébert, J. Van Herle, A. Hessler-Wyser, J. Mater. Sci. **48**, 2893-2907 (2013).

[18] K.V. Manukyan, A. Avetisyan, C. Shuck, H. Chatilyan, S. Rouvimov, S. Kharatyan, A.S. Mukasyan, J. Phys. Chem. C. **119**, 16131-16138 (2015).

[19] J.A. Rodriguez, J.C. Hanson, A.I. Frenkel, J.Y. Kim, M. Pérez, J. Am. Chem. Soc. **124**, 346-354 (2002).

[20] A. Khawam, D.R. Flanagan, J. Phys. Chem. B. **110**, 17315-17328 (2006).

[21] B.V. L'vov, Russ. J. Appl. Chem. **83**, 728-736 (2010).

[22] D.K. Kuhn, H.H. Johnson, Acta Metall. Mater. **39**, 2901-2908 (1991).

[23] S.P. Zholobov, M.D. Malev, Zh. Tekh. Fiz. **41**, 677 (1971).

[24] A. Atkinson, R.I. Taylor, Phil. Mag. A, **39**, 581-595 (1979).